Interband Pairing as the Origin of the Sublattice Dichotomy in Monolayer FeSe/$SrTiO_3$

Zhipeng Xu[1,2], Shengshan Qin[3*], Kun Jiang[1,2*], and Jiangping Hu[1,4,5*]

[1]*Beijing National Laboratory for Condensed Matter Physics and Institute of Physics, Chinese Academy of Sciences, Beijing 100190, China*
[2]*School of Physical Sciences, University of Chinese Academy of Sciences, Beijing 100190, China*
[3]*School of Physics, Beijing Institute of Technology, Beijing 100081, China*
[4]*Kavli Institute of Theoretical Sciences, University of Chinese Academy of Sciences, Beijing 100190, China*
[5]*New Cornerstone Science Laboratory, Beijing 100190, China*

(Received 15 November 2025; accepted manuscript online 29 December 2025)

Sublattice dichotomy in monolayer FeSe/$SrTiO_3$, signaling the breaking of symmetries exchanging the two Fe sublattices, has recently been reported. We propose that interband pairing serves as the origin of this dichotomy, regardless of whether the symmetries are broken in the normal state or in the pairing state. If symmetry breaking occurs in the normal state, the Fermi surfaces are sublattice-polarized, and the intersublattice d-wave pairing naturally acts as interband pairing, reproducing the observed dichotomy in the spectra. Alternatively, if symmetry breaking takes place in the pairing state, the dichotomy arises from the coexistence of intraband and interband pairing, with the constraint that interband pairings share the same sign while intraband pairings carry opposite signs. In both cases, interband pairing is indispensable, establishing it as a key ingredient for understanding superconductivity in monolayer FeSe/$SrTiO_3$.

DOI: 10.1088/0256-307X/43/2/020707 CSTR: 32039.14.0256-307X.43.2.020707

1. Introduction. Iron-based superconductors have attracted sustained and widespread interest since their initial discovery,[1–10] owing to their high critical temperatures, rich phase diagrams,[3,4,11–14] and unconventional pairing mechanisms.[1,2,15–18] Among these materials, a particularly striking development was the discovery of a record-high superconducting transition temperature (∼65 K) in monolayer FeSe films grown on $SrTiO_3$ substrate.[19–26] This system differs fundamentally from the usual iron pnictides. Angle-resolved photoemission spectroscopy (ARPES) measurements reveal that the hole-like bands near the Γ point are below the Fermi level, leaving only electron pockets at the Brillouin zone corner.[27] The absence of the hole pockets invalidates the Fermi surface nesting scenario commonly invoked in the iron-based superconductors.[15,16] Therefore, monolayer FeSe/$SrTiO_3$ has become a unique platform for exploring unconventional, interface-enhanced high-T_c superconductivity.[28–32]

The monolayer FeSe consists of a single layer of Fe atoms arranged in a square lattice, sandwiched by two Se atomic layers positioned alternately above (Se^+) and below (Se^-) the Fe plane [see Fig. 1(a)]. The alternating positioning of the Se atoms above and below the Fe plane doubles the size of the structural unit cell of the Fe square lattice, resulting in two Fe atoms per unit cell, named Fe_A and Fe_B. For the pristine monolayer FeSe, these two sublattices are equivalent to each other due to symmetries, such as inversion symmetry whose center locates at the middle of the Fe_A-Fe_B bond. In the material, however, the existence of substrate, electronic ordering, and many other issues may break the equivalence of the two sublattices.

Recently, sublattice dichotomy has been witnessed in the monolayer FeSe/$SrTiO_3$ in a scanning tunneling microscopy and spectroscopy (STM/STS) experiment.[33] Distinct dual tunneling spectra within the pairing gap corresponding to the two Fe sublattices [schematically illustrated in Fig. 1(b)] are observed. Specifically, two superconducting gaps are identfied, namely V_i and V_o. The coherence peak at $+V_\mathrm{i}$ on Fe_A is lower than that on Fe_B, whereas the coherence peak at $-V_\mathrm{i}$ on Fe_A is higher. Conversely, the intensity difference of the coherence peaks at $\pm V_\mathrm{o}$ exhibits the opposite behavior. This intriguing phenomenon is reminiscent of interband pairing[35–39] in multiband superconductors. The interband pairing describes Cooper pairs formed by electrons from bands with different masses, as illustrated in Fig. 1(c). Since the particle and hole sectors forming the Cooper pair are from the bands with distinct masses, such a subsystem intrinsically lacks particle–hole symmetry. Accordingly, the pairing between them necessarily produces particle–hole asymmetric spectra.[35] Density of states (DOS) projected onto each band for a two-band superconductor with interband pairing are calculated in Ref. [35] and also presented here in Fig. 1(d). As shown, the coherence peaks of band 1 shift

*Corresponding authors. Email: qinshengshan@bit.edu.cn; jiangkun@iphy.ac.cn; jphu@iphy.ac.cn
© 2026 Chinese Physical Society and IOP Publishing Ltd. All rights, including for text and data mining, AI training, and similar technologies, are reserved.

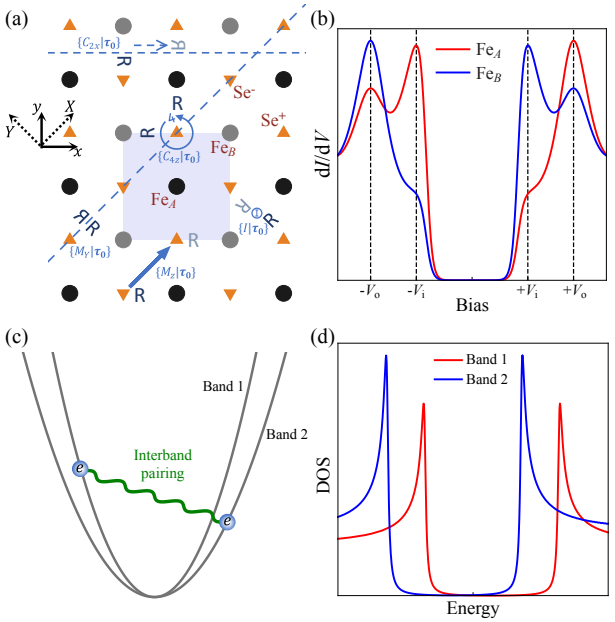

Fig. 1. (a) (Left) Coordinate systems used in this paper. (Right) Top view of monolayer FeSe. Fe atoms are depicted with solid circles in black and gray, corresponding to the two Fe sublattices. Se atoms above and below the Fe plane are represented by upward-pointing and downward-pointing filled triangles, respectively. Fe_A, Fe_B, Se^+ and Se^- are the notations for each type of atom. A single unit cell is indicated by the shaded square region. Symmetries exchanging the two Fe sublattices, $\{I|\boldsymbol{\tau_0}\}$, $\{C_{4z}|\boldsymbol{\tau_0}\}$, $\{M_Y|\boldsymbol{\tau_0}\}$, $\{M_z|\boldsymbol{\tau_0}\}$, and $\{C_{2x}|\boldsymbol{\tau_0}\}$ where $\boldsymbol{\tau_0} = (1/2, 1/2)$, are depicted in blue, with paired "R" symbols visualizing the symmetry action—each pair represents the original object and its image under the corresponding operation. The dark blue "R" is above the Fe plane, and the light blue one is below. The name of each symmetry is indicated nearby.[34] (b) Schematic of the observed tunneling spectra on two sublattices. V_i and V_o are the inner and outer gaps. (c) Schematic of interband pairing. (d) DOS projected onto each band for a two-band superconductor with interband pairing.[35]

positively by half the energy difference between the two bands, while those of band 2 shift negatively by the same amount. Though the above analyses refer to the band-projected DOS in a two-band superconductor, the resulting spectra closely resemble the experimentally observed ones, i.e., the sublattice-projected DOS as displayed in Figs. 1(b) and 1(d). Therefore, we propose that interband pairing underlies the sublattice dichotomy.

This paper is organized as follows. Section 2 is devoted to the symmetry analysis, which identifies the symmetry requirement for realizing the sublattice dichotomy. Sections 3 and 4 discuss two cases: symmetry breaking in the normal state and in the pairing state, both of which emphasize the role of interband pairing. Section 4 is for summary and discussion.

2. Symmetry Analysis. To figure out the origin of the sublattice dichotomy in monolayer $FeSe/SrTiO_3$, we start with a symmetry analysis. The pristine monolayer FeSe respects the space group $G = P4/nmm$, which is nonsymmorphic. Its quotient group $G/\mathcal{T}$ with $\mathcal{T}$ being the translation subgroup contains 16 symmetry operations as listed in Table 1, the point group part of which is isomorphic to the point group D_{4h}. The symmetry operations in $G/\mathcal{T}$ can be classified into two categories; Half of the symmetry operations map the Fe_A sublattice to the Fe_B sublattice, and the others does not exchange the two Fe sublattices. We list the two categories of symmetry operations in Table 1, and schematically illustrate the symmetries exchanging the two Fe sublattices in Fig. 1(a). Here, we use the Seitz notation $\{g|\boldsymbol{\tau}\}$ where g is a point group operation and $\boldsymbol{\tau}$ is a translation, to describe the symmetry operations.

Due to the symmetries exchanging the two Fe sublattices, it is natural to expect exactly the same experimental observations at Fe_A and Fe_B in the monolayer $FeSe/SrTiO_3$. Conversely, the sublattice dichotomy observed in recent experiments unambiguously indicates that all the symmetry operations mapping Fe_A to Fe_B are broken. To realize such a condition, orders belonging to different irreducible representations must be present. Notably, in the Nambu basis the BdG Hamiltonian of a superconductor always belongs to the A_{1g} irreducible representation, if only one single pairing order is considered, regardless of the specific pairing symmetry. Hence, according to Table 1, the problem reduces to identifying a B_{2u} perturbation to the BdG Hamiltonian. Notice that the B_{2u} perturbations can be the superconducting pairing orders or the orders in the normal bands.

Table 1. Character table of $G/\mathcal{T}$ (isomorphic to D_{4h}), where $\boldsymbol{\tau_0}$ stands for the translation $(1/2, 1/2)$. The symmetry operations that exchange the two Fe sublattices are listed in the right half.

	$\{E\|\mathbf{0}\}$	$2\{S_{4z}\|\mathbf{0}\}$	$\{C_{2z}\|\mathbf{0}\}$	$\{C_{2\,X/Y}\|\mathbf{0}\}$	$\{M_{x/y}\|\mathbf{0}\}$	$\{I\|\boldsymbol{\tau_0}\}$	$2\{C_{4z}\|\boldsymbol{\tau_0}\}$	$\{M_{X/Y}\|\boldsymbol{\tau_0}\}$	$\{M_z\|\boldsymbol{\tau_0}\}$	$\{C_{2\,x/y}\|\boldsymbol{\tau_0}\}$
A_{1g}	1	1	1	1	1	1	1	1	1	1
A_{2g}	1	1	1	−1	−1	1	1	−1	1	−1
B_{1g}	1	−1	1	−1	1	1	−1	−1	1	1
B_{2g}	1	−1	1	1	−1	1	−1	1	1	−1
E_g	2	0	−2	0	0	2	0	0	−2	0
A_{1u}	1	−1	1	1	−1	−1	1	−1	−1	1
A_{2u}	1	−1	1	−1	1	−1	1	1	−1	−1
B_{1u}	1	1	1	−1	−1	−1	−1	1	−1	1
B_{2u}	1	1	1	1	1	−1	−1	−1	−1	−1
E_u	2	0	−2	0	0	−2	0	0	2	0

3. Normal State Symmetry Breaking. We first consider the symmetries are broken in the normal state. We adopt the low-energy $k \cdot p$ model developed in Ref. [34], which resembles the electron pockets near the Brillouin zone corner, i.e., the M point, in the monolayer FeSe/SrTiO$_3$.[27,33] The model respects the full symmetries of the space group $P4/nmm$, and takes the form $H_0 = \sum_{\boldsymbol{k},\sigma} \psi^\dagger_\sigma(\boldsymbol{k}) h_M(\boldsymbol{k}) \psi_\sigma(\boldsymbol{k})$ with

$$h_M(\boldsymbol{k}) = \begin{pmatrix} h^+_M(\boldsymbol{k}) & 0 \\ 0 & h^-_M(\boldsymbol{k}) \end{pmatrix}, \tag{1a}$$

where

$$h^\pm_M(\boldsymbol{k}) = \begin{pmatrix} \epsilon_1 + \frac{\boldsymbol{k}^2}{2m_1} \pm a_1 k_x k_y & -\mathrm{i}v_\pm(\boldsymbol{k}) \\ \mathrm{i}v_\pm(\boldsymbol{k}) & \epsilon_3 + \frac{\boldsymbol{k}^2}{2m_3} \pm a_3 k_x k_y \end{pmatrix}, \tag{1b}$$

and

$$\begin{aligned} v_\pm(\boldsymbol{k}) &= v(\pm k_x + k_y) \\ &\quad + p_1(\pm k_x^3 + k_y^3) + p_2 k_x k_y (k_x \pm k_y). \end{aligned} \tag{1c}$$

The above Hamiltonian is written in the d-orbital basis

$$\psi_\sigma(\boldsymbol{k}) = \frac{1}{\sqrt{2}} \begin{pmatrix} d^A_{Xz,\sigma}(\boldsymbol{k}) - d^B_{Xz,\sigma}(\boldsymbol{k}) \\ d^A_{XY,\sigma}(\boldsymbol{k}) + d^B_{XY,\sigma}(\boldsymbol{k}) \\ d^A_{Yz,\sigma}(\boldsymbol{k}) + d^B_{Yz,\sigma}(\boldsymbol{k}) \\ d^A_{XY,\sigma}(\boldsymbol{k}) - d^B_{XY,\sigma}(\boldsymbol{k}) \end{pmatrix}, \tag{2}$$

where $\boldsymbol{k}$ is measured from the M point, σ is the spin index, and A (B) stands for the Fe$_A$ (Fe$_B$) sublattice.

We use the above model to fit the experimentally reported Fermi surfaces of the monolayer FeSe/SrTiO$_3$,[33] and derive the parameters as $\epsilon_1 = -95.00$, $\epsilon_3 = -60.00$, $1/2m_1 = -2.40$, $1/2m_3 = 20.58$, $a_1 = 38.06$, $a_3 = -48.56$, $v = 39.90$, $p_1 = -0.63$, and $p_2 = -1.87$, which are all in unit of meV. The corresponding Fermi surfaces showing the sublattice weight are presented in Fig. 2(a). As shown in the figure, on the Fermi surfaces the two sublattices are evenly mixed. This arises from the constraint imposed by the glide-mirror symmetry $\{M_z|\boldsymbol{\tau_0}\}$ which exchanges the two Fe sublattices but leaves $\boldsymbol{k}$ invariant.

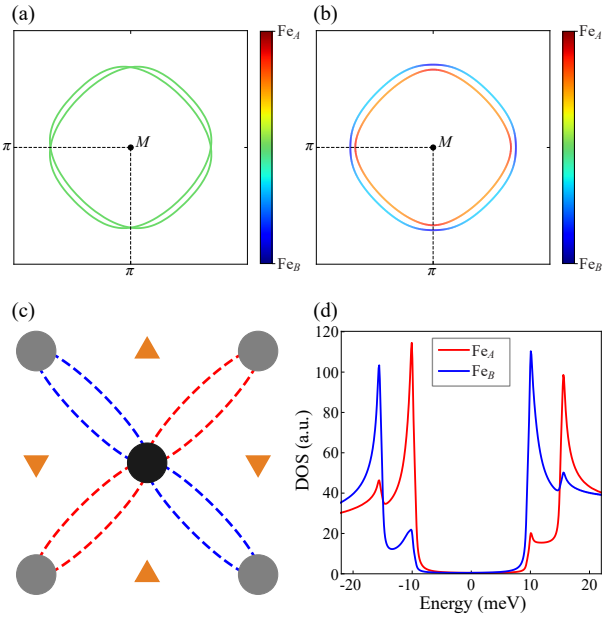

Fig. 2. (a) Fermi surfaces without symmetry-breaking terms. Parameters are taken as $\epsilon_1 = -95.00$, $\epsilon_3 = -60.00$, $1/2m_1 = -2.40$, $1/2m_3 = 20.58$, $a_1 = 38.06$, $a_3 = -48.56$, $v = 39.90$, $p_1 = -0.63$, and $p_2 = -1.87$ in unit of meV to mimic the experimental Fermi surface results.[33] (b) Fermi surfaces with symmetry-breaking terms. Parameters in $h'_M(\boldsymbol{k})$ are taken as $v_1 = v_2 = v_3 = v_4 = 1.00$ meV. The color in (a) and (b) represents the sublattice weight. (c) Schematic illustration of nodeless d-wave pairing in real space. The pairing is positive (red) in the X-direction and negative (blue) in the Y-direction. (d) Calculated DOS with the combination of normal state symmetry breaking Eq. (3) and nodeless d-wave pairing Eq. (4), where $\Delta_\mathrm{d} = 12.20$ meV.

Based on the low-energy effective model, we now consider perturbations that break all the symmetries exchanging the two Fe sublattices, i.e., the B_{2u} perturbations in the normal bands. Note that the B_{2u} perturbations in the normal state must also be the B_{2u} perturbations in the superconducting state. Under the basis in Eq. (2), up to the $\boldsymbol{k}^2$ order the perturbations take the form

$$h'_M(\boldsymbol{k}) = \begin{pmatrix} 0 & 0 & v_3(k_x^2 - k_y^2) & -\mathrm{i}v_4(k_x + k_y) \\ 0 & 0 & \mathrm{i}v_4(-k_x + k_y) & v_1 + v_2\boldsymbol{k}^2 \\ v_3(k_x^2 - k_y^2) & -\mathrm{i}v_4(-k_x + k_y) & 0 & 0 \\ \mathrm{i}v_4(k_x + k_y) & v_1 + v_2\boldsymbol{k}^2 & 0 & 0 \end{pmatrix}. \tag{3}$$

Upon adding h'_M into h_M with $v_1 = v_2 = v_3 = v_4 = 1.00$ meV, the corresponding Fermi surfaces are shown in Fig. 2(b). The sublattice weights are clearly redistributed; Specifically, the inner Fermi surface is predominantly contributed by Fe$_A$, while the outer one is mainly from Fe$_B$. The results suggest a correspondence between the sublattices and the bands. Thus, the intersublattice pairing effectively plays the role of the interband pairing, potentially giving rise to the features of Fig. 1(d). In the intersublattice pairing channel, the s-wave pairing gives nodal superconducting state. Considering the nodeless superconducting gap observed in the monolayer FeSe/SrTiO$_3$, we focus on the intersublattice d-wave pairing,[40–43] more specifically the d-wave pairing between the nearest-neighbor Fe$_A$ and Fe$_B$ sites. The d-wave pairing order changes sign under the S_4 symmetry as schematically illustrated in Fig. 2(c). As the Fermi surfaces are located around M which is S_4 invariant, superconducting nodes should have existed on the Fermi surfaces; However, due to the interband pairing nature of the intersublattice pairing, the d-wave pairing state is actually fully gapped.

The leading order of the nodeless d-wave pairing,

expressed in form of $\psi^\dagger_\uparrow(\boldsymbol{k})\Delta(\boldsymbol{k})[\psi^\dagger_\downarrow(-\boldsymbol{k})]^T$, is given by

$$\Delta(\boldsymbol{k}) = \Delta_{\rm d}\begin{pmatrix}1&0&0&0\\0&1&0&0\\0&0&-1&0\\0&0&0&-1\end{pmatrix}. \tag{4}$$

Combining the normal-state perturbations in Eq. (3) and the nodeless d-wave pairing in Eq. (4), we calculate the DOS at Fe_A and Fe_B, and the results are presented in Fig. 2(d). As expected, the sublattice dichotomy of the superconducting coherence peaks is realized, due to the sublattice-polarized Fermi surfaces and the interband nature of the d-wave pairing.

Before ending this part, we note that incorporating the $s_\pm$ pairing component, alongside the above d-wave pairing, does not necessarily alter the sublattice dichotomy, provided that the magnitude of $s_\pm$ component is not dominant.

4. Pairing State Symmetry Breaking. The sublattice dichotomy in the monolayer FeSe/$SrTiO_3$ may also arise from the mix of the different pairing orders. To break the symmetries mapping Fe_A to Fe_B, according to Table 1, one need to consider the following pairing combinations, $A_{1g}+B_{2u}$, $A_{2g}+B_{1u}$, $B_{1g}+A_{2u}$, and $B_{2g}+A_{1u}$. Here, we focus on the pairings belonging to the 1D irreducible representations. In fact, for each of the above pairing combinations, if we consider the even-parity (odd-parity) order separately the system is invariant under the crystalline symmetries, i.e., the BdG Hamiltonian belonging to the A_{1g} irreducible representation, and the odd-parity (even-parity) order serves as the B_{2u} perturbations in the sense of the BdG Hamiltonian.

For the iron-based superconductors, it has been revealed[44] that for the 1D irreducible representations the even-parity pairing orders correspond to intraband pairing, whereas the odd-parity orders correspond to interband pairing. To obtain the sublattice dichotomy in the monolayer FeSe/$SrTiO_3$, the coexistence of intraband and interband pairing serves as the starting point, and additional constraints on their relative phases must be imposed as we shall show in the following.

Before considering the monolayer FeSe/$SrTiO_3$, it is helpful to utilize a simple two-band model to develop some insights. We denote the band operators as $c^\dagger_{1k\sigma}$ and $c^\dagger_{2k\sigma}$, and assume simple dispersions $\gamma_1 k^2-\mu$ and $\gamma_2 k^2-\mu$ ($\gamma_1>\gamma_2$) for the two bands. The BdG Hamiltonian under the basis $\Psi^\dagger_k=(c^\dagger_{1k\uparrow},c^\dagger_{2k\uparrow},c_{1,-k\downarrow},c_{2,-k\downarrow})$ is

$$H_{\rm BdG}=\begin{pmatrix}\gamma_1k^2-\mu&0&\Delta_{a1}&\Delta_{b1}\\0&\gamma_2k^2-\mu&\Delta_{b2}&\Delta_{a2}\\\Delta^*_{a1}&\Delta^*_{b2}&-\gamma_1k^2+\mu&0\\\Delta^*_{b1}&\Delta^*_{a2}&0&-\gamma_2k^2+\mu\end{pmatrix}, \tag{5}$$

where $\Delta_{a1(2)}$ and $\Delta_{b1(2)}$ are the intraband and interband pairings, respectively. To determine the conditions under which the sublattice dichotomy emerges, we perform a perturbation analysis (details in the Supplementary Materials) and find that the only pairing configuration yielding the sublattice dichotomy is $\Delta_{b1}=\Delta_{b2}$ and $\Delta_{a1}=-\Delta_{a2}$, i.e., the interband pairing having the same sign and the intraband pairing having opposite signs.

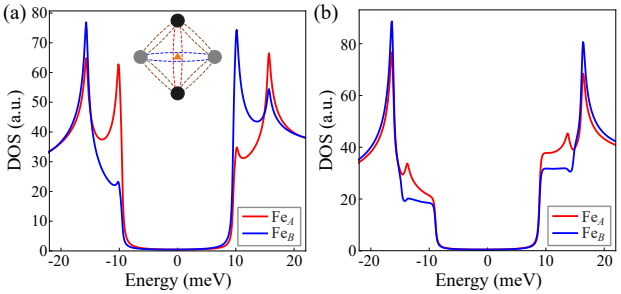

Fig. 3. Calculated DOSs with pairing combinations of (a) Eq. (6) with (7b), (b) Eq. (6) with (7a). Parameters are (a) $\Delta_{b2u}=15\,$meV, $\Delta_{a1g}=10\,$meV; (b) $\Delta_{b2u}=18\,$meV, $\Delta_{a1g}=-0.5\,$meV. The inset in (a) is the schematic illustration of the pairing combination of Eq. (6) with (7b) in real space. The intrasublattice pairing is positive (red) on Fe_A-Fe_A bonds and negative (blue) on Fe_B-Fe_B bonds, while all intersublattice pairings share the same sign (brown).

We examine the above criterion in the monolayer FeSe/$SrTiO_3$. Specifically, we consider the pairings $A_{1g}+B_{2u}$ as an example in the $k\cdot p$ model in Eq. (1a). The leading order of the B_{2u} pairing under the basis in Eq. (2) is

$$B_{2u}:\Delta(\boldsymbol{k})=\Delta_{b2u}\begin{pmatrix}0&0&0&0\\0&0&0&1\\0&0&0&0\\0&1&0&0\end{pmatrix}. \tag{6}$$

Based on the $k\cdot p$ in Eq. (1a), it can be found the B_{2u} pairing in Eq. (6) is actually the pure interband pairing which occurs in the d_{XY} orbital. Moreover, the B_{2u} pairing in Eq. (6) is even with respect to the band indices, satisfying the criterion for the sublattice dichotomy. For the A_{1g} pairing, the two leading orders preserved up to $\boldsymbol{k}^2$ take the form

$$A_{1g}:\Delta(\boldsymbol{k})=\Delta_{a1g}\begin{pmatrix}1&0&0&0\\0&1&0&0\\0&0&1&0\\0&0&0&1\end{pmatrix}, \tag{7a}$$

$$A_{1g}:\Delta(\boldsymbol{k})=\Delta_{a1g}\begin{pmatrix}k_xk_y&0&0&0\\0&k_xk_y&0&0\\0&0&-k_xk_y&0\\0&0&0&-k_xk_y\end{pmatrix}. \tag{7b}$$

Based on the criterion developed in the above, only the A_{1g} pairing in Eq. (7b) which is odd with respect to the band indices satisfies the condition. We further simulate the superconducting DOSs with the B_{2u} pairing in Eq. (6) and the A_{1g} pairing in Eq. (7b), and present the results in Fig. 3(a). As expected, the sublattice dichotomy is observed at the Fe_A and Fe_B sites, consistent with the experiments. To compare, we also calculate the case with the B_{2u} pairing in Eq. (6) and the A_{1g} pairing in Eq. (7a); as shown in Fig. 3(b), no sublattice dichotomy appears.

In real space, for the above pairing combination responsible for the sublattice dichotomy, the B_{2u} order in

Eq. (6) corresponds to the nearest-neighbour intrasublattice pairing which is S_4 invariant but have opposite signs in the Fe_A sublattice and Fe_B sublattice; while the A_{1g} order in Eq. (7b) describes the nearest-neighbour intersublattice pairing with a uniform pairing sign. We schematically illustrate the two pairing orders in the inset of Fig. 3(a). Such a pairing combination has been proposed in Ref. [44].

5. Summary and Discussion. In summary, we have identified interband pairing as a key ingredient in understanding the sublattice dichotomy observed in the monolayer FeSe/$SrTiO_3$.[33] Two possibilities are recognized for such symmetry-breaking. In the first case, symmetry-breaking is present in the normal state, leading to sublattice-polarized Fermi surfaces. The intersublattice d-wave pairing effectively acts as interband pairing, which can naturally reproduce the experimentally observed dichotomy in the spectra. However, we notice that the nodeless d-wave pairing is challenged by vortex-core STM/STS measurements,[45] which report a CdGM spectrum inconsistent with d-wave–based theoretical predictions.[46] This discrepancy calls further explorations. In the second case, symmetry breaking emerges at the superconducting level through one of the four possible pairing combinations: $A_{1g}+B_{2u}$, $A_{2g}+B_{1u}$, $B_{1g}+A_{2u}$, and $B_{2g}+A_{1u}$, which corresponds to the coexistence of both intraband and interband pairing. Here, an additional constraint is required to realize the sublattice dichotomy: while the interband pairings must share the same sign, the intraband pairings must carry opposite signs.

During the preparation of this manuscript, we became aware of Ref. [47], which also investigates the origin of the sublattice dichotomy in monolayer FeSe/$SrTiO_3$, reaching broadly consistent physical conclusions. Our study, however, differs from Ref. [47] in several aspects. First, we highlight that interband pairing serves as the key ingredient irrespective of whether the symmetry breaking takes place in the normal state or in the pairing state. Second, we employ a three-orbital model from fitting experimental observations in comparison to the simplified model used in Ref. [47]. Third, we perform a general analysis for the pairing combination case and identify a necessary sign constraint on the intraband and interband pairing components.

Acknowledgments. This work was supported by the Ministry of Science and Technology (Grant No. 2022YFA1403900), the National Natural Science Foundation of China (Grant Nos. 12494594, 12174428, and 12304163), the New Cornerstone Investigator Program, the Chinese Academy of Sciences Project for Young Scientists in Basic Research (Grant No. 2022YSBR-048), and the Beijing Institute of Technology Research Fund Program for Young Scholars.

References

[1] Hirschfeld P J, Korshunov M M, and Mazin I I 2011 *Rep. Prog. Phys.* **74** 124508
[2] Chubukov A 2012 *Annu. Rev. Condens. Matter Phys.* **3** 57
[3] Si Q, Yu R, and Abrahams E 2016 *Nat. Rev. Mater.* **1** 16017
[4] Fernandes R M, Coldea A I, Ding H, Fisher I R, Hirschfeld P J, and Kotliar G 2022 *Nature* **601** 35
[5] Kamihara Y, Watanabe T, Hirano M, and Hosono H 2008 *J. Am. Chem. Soc.* **130** 3296
[6] Rotter M, Tegel M, and Johrendt D 2008 *Phys. Rev. Lett.* **101** 107006
[7] Hsu F C, Luo J Y, Yeh K W, Chen T K, Huang T W, Wu P M, Lee Y C, Huang Y L, Chu Y Y, Yan D C, and Wu M K 2008 *Proc. Natl. Acad. Sci. U.S.A.* **105** 14262
[8] Tapp J H, Tang Z, Lv B, Sasmal K, Lorenz B, Chu P C W, and Guloy A M 2008 *Phys. Rev. B* **78** 060505
[9] Wang X, Liu Q, Lv Y, Gao W, Yang L, Yu R, Li F, and Jin C 2008 *Solid State Commun.* **148** 538
[10] Guo J, Jin S, Wang G, Wang S, Zhu K, Zhou T, He M, and Chen X 2010 *Phys. Rev. B* **82** 180520
[11] Fernandes R M, Chubukov A V, and Schmalian J 2014 *Nat. Phys.* **10** 97
[12] Fernandes R M and Chubukov A V 2016 *Rep. Prog. Phys.* **80** 014503
[13] Dai P 2015 *Rev. Mod. Phys.* **87** 855
[14] Böhmer A E and Kreisel A 2017 *J. Phys.: Condens. Matter* **30** 023001
[15] Mazin I I, Singh D J, Johannes M D, and Du M H 2008 *Phys. Rev. Lett.* **101** 057003
[16] Kuroki K, Onari S, Arita R, Usui H, Tanaka Y, Kontani H, and Aoki H 2008 *Phys. Rev. Lett.* **101** 087004
[17] Seo K, Bernevig B A, and Hu J 2008 *Phys. Rev. Lett.* **101** 206404
[18] Fang C, Wu Y L, Thomale R, Bernevig B A, and Hu J 2011 *Phys. Rev. X* **1** 011009
[19] Wang Q Y, Li Z, Zhang W H, Zhang Z C, Zhang J S, Li W, Ding H, Ou Y B, Deng P, Chang K, Wen J, Song C L, He K, Jia J F, Ji S H, Wang Y Y, Wang L L, Chen X, Ma X C, and Xue Q K 2012 *Chin. Phys. Lett.* **29** 037402
[20] He S, He J, Zhang W, Zhao L, Liu D, Liu X, Mou D, Ou Y B, Wang Q Y, Li Z, Wang L, Peng Y, Liu Y, Chen C, Yu L, Liu G, Dong X, Zhang J, Chen C, Xu Z, Chen X, Ma X, Xue Q, and Zhou X 2013 *Nat. Mater.* **12** 605
[21] Tan S, Zhang Y, Xia M, Ye Z, Chen F, Xie X, Peng R, Xu D, Fan Q, Xu H, Jiang J, Zhang T, Lai X, Xiang T, Hu J, Xie B, and Feng D 2013 *Nat. Mater.* **12** 634
[22] Lee J J, Schmitt F T, Moore R G, Johnston S, Cui Y T, Li W, Yi M, Liu Z K, Hashimoto M, Zhang Y, Lu D H, Devereaux T P, Lee D H, and Shen Z X 2014 *Nature* **515** 245
[23] Zhang Z, Wang Y H, Song Q, Liu C, Peng R, Moler K, Feng D, and Wang Y 2015 *Sci. Bull.* **60** 1301
[24] Ge J F, Liu Z L, Liu C, Gao C L, Qian D, Xue Q K, Liu Y, and Jia J F 2015 *Nat. Mater.* **14** 285
[25] Huang D and Hoffman J E 2017 *Annu. Rev. Condens. Matter Phys.* **8** 311
[26] Xu Y, Rong H, Wang Q, Wu D, Hu Y, Cai Y, Gao Q, Yan H, Li C, Yin C, Chen H, Huang J, Zhu Z, Huang Y, Liu G, Xu Z, Zhao L, and Zhou X J 2021 *Nat. Commun.* **12** 2840
[27] Liu D, Zhang W, Mou D, He J, Ou Y B, Wang Q Y, Li Z, Wang L, Zhao L, He S, Peng Y, Liu X, Chen C, Yu L, Liu G, Dong X, Zhang J, Chen C, Xu Z, Hu J, Chen X, Ma X, Xue Q, and Zhou X 2012 *Nat. Commun.* **3** 931
[28] Fan Q, Zhang W H, Liu X, Yan Y J, Ren M Q, Peng R, Xu H C, Xie B P, Hu J P, Zhang T, and Feng D L 2015 *Nat. Phys.* **11** 946
[29] Chen X, Maiti S, Linscheid A, and Hirschfeld P J 2015 *Phys. Rev. B* **92** 224514
[30] Huang D, Webb T A, Fang S, Song C L, Chang C Z, Moodera J S, Kaxiras E, and Hoffman J E 2016 *Phys. Rev. B* **93** 125129
[31] Linscheid A, Maiti S, Wang Y, Johnston S, and Hirschfeld P J 2016 *Phys. Rev. Lett.* **117** 077003

[32] Zhang Y, Lee J J, Moore R G, Li W, Yi M, Hashimoto M, Lu D H, Devereaux T P, Lee D H, and Shen Z X 2016 *Phys. Rev. Lett.* **117** 117001
[33] Ding C, Xu Z, Jiao X, Hu Y, Zhao W, Yang L, Jiang K, Wang L, Jia J F, Hu J, and Xue Q K 2024 arXiv:2406.15239 [cond-mat.supr-con]
[34] Cvetkovic V and Vafek O 2013 *Phys. Rev. B* **88** 134510
[35] Li P, Jiang K, and Hu J 2024 *Phys. Rev. B* **110** 094517
[36] Mei J, Qin S, and Hu J 2025 arXiv:2510.15788 [cond-mat.supr-con]
[37] Moreo A, Daghofer M, Nicholson A, and Dagotto E 2009 *Phys. Rev. B* **80** 104507
[38] Tahir-Kheli J 1998 *Phys. Rev. B* **58** 12307
[39] Dolgov O V, Fetisov E P, Khomskii D I, and Svozil K 1987 *Z. Physik B - Condensed Matter* **67** 63
[40] Agterberg D F, Shishidou T, O'Halloran J, Brydon P M R, and Weinert M 2017 *Phys. Rev. Lett.* **119** 267001
[41] Maier T A, Graser S, Hirschfeld P J, and Scalapino D J 2011 *Phys. Rev. B* **83** 100515
[42] Mazin I I 2011 *Phys. Rev. B* **84** 024529
[43] Kreisel A, Wang Y, Maier T A, Hirschfeld P J, and Scalapino D J 2013 *Phys. Rev. B* **88** 094522
[44] Hu J 2013 *Phys. Rev. X* **3** 031004
[45] Chen C, Liu Q, Bao W C, Yan Y, Wang Q H, Zhang T, and Feng D 2020 *Phys. Rev. Lett.* **124** 097001
[46] Xiang K, Wang D, and Wang Q 2025 *Progress in Physics* **45** 250
[47] Roig M, Islam K R, Oli B D, Zhang H, Brydon P, Ramires A, Yu Y, Weinert M, Li L, and Agterberg D F 2025 arXiv:2511.02226